Spectral Noise Analysis of a CMOS Imager at Low Temperature for Logarithmic Mode

Aldemir Silva Teixeira, Jr., Eduardo Adriano Cotta, Carlos Augusto de Moraes Cruz, *Member, IEEE*, and Davies William de Lima Monteiro, *Member, IEEE*

***Abstract*— The most common and useful CMOS high-dynamic-range imager is the one employing the active pixel sensor (APS) operating in the logarithmic mode. Notwithstanding, temporal noise can compromise the quality of the image generated by the focal-plane array. Most of the image-sensor noise models and results found in the literature are limited to a temperature range higher than that of the freezeout temperature, where the semiconductor doping impurities are all activated. The focus of this paper is to compare the noise spectrum behavior of the logarithmic image sensor at room temperature with that of a temperature near and below the freezeout point. Experimental results carried out in a small bidimensional pixel array fabricated in a standard 4-metal 2-poly 0.35-μm CMOS technology suggests that thermal noise remains quite steady as the temperature reduces due to the increase in the sense-node resistance of the pixel circuitry. On the other hand, "spikes" have been identified with significant intensity in the spectral noise in all pixels when studied individually. These spikes in the spectrum have the same value in frequency when the device is submitted to different light intensities and temperatures. However, they were only observed for temperatures below 150 K and for frequencies below the corner frequency. The nonrandomic presence of these spikes in the noise spectrum indicates the presence of traps related to the defects inside the gate oxide and at the oxide–silicon interface. At room temperature, these spikes are not observed due to the thermal energy being higher than the binding energy of these traps.**

***Index Terms*— Active pixel sensor (APS), CMOS image sensor (CIS), freezeout temperature, high dynamic range (HDR), power spectrum density, spikes, temporal spectrum noise.**

I. Introduction

DUE to its adequate functionality and circuitry simplicity, the basic three-FET active pixel sensor (APS) operating in the logarithmic mode is one of the preferred choices for high-dynamic-range CMOS image sensors (HDR CISs). Besides operation in applications demanding HDR [1], [2] such as assistive on board vision, monitoring of reflecting surfaces, and laser welding inspection; APS circuits can be tailored to a broad range of deployments, including 3-D imaging, high-speed imaging capture, aerospace imaging, photon counting [3], attending to many more consumer, industrial, and scientific needs.

However, it is often necessary that the device presents a substantial reduction of the temporal and spatial noise. The main application for noise reduction is present on read out integrated circuits (ROICs) designed for quantum-dot infrared photodetector (QDIP) or quantum-well infrared photodetector (QWIP) arrays in which low readout noise is necessary to differentiate between the background and the scene of interest. A traditional process for noise suppression in these devices includes signal-processing circuits, which uses the correlated double sampling (CDS) technique [4], and submit the sensor at low temperatures using Peltier thermal coolers. The temperature reduction prevents the thermal generation of charge carriers, and competes with the optical ones, making noncooled devices very noisy. Thus, the submission of these devices to cryogenic temperatures can lead to a large signal-to-noise ratio (SNR) in HDR, in principle.

In the literature, there are a vast number of references presenting techniques to remove or minimize the spatial noise [4]–[8], also known as fixed pattern noise (FPN). Methods to suppress temporal noise, on the other hand, are much less reported, especially because it has several underlying contributions, of which the main ones are the shot and thermal mechanisms, whose effects are inherent either to the light source or to the carrier dynamics in the material. These mechanisms can be minimized by operating the image sensor at cryogenic temperatures (i.e., below 150 K), where, in principle, they can be significantly suppressed. However, at those temperatures (or below the freezeout temperature for the doped

Manuscript received October 26, 2018; revised January 21, 2019; 2911008accepted April 10, 2019. This work was supported in part by INCT:DISSE, in part by CNPq for manufacturing the sensor, in part by the Coordenação de Aperfeiçoamento de Pessoal de Nível Superior—Brasil (CAPES)—Finance Code 001, CNPq, and FINEP to enable chip manufacturing, infrastructure, equipment, and grants, in part by FAPEAM, in part by FAPEMIG, in part by Programa de Pós-Graduação em Engenharia Elétrica da/UFMG (PPGEE/UFMG), in part by Programa de Pós-Graduação em Engenharia Elétrica da/UFAM (PPGEE/UFAM), in part by Pró-Reitoria de Pesquisa da/UFMG (PRPq/UFMG), and in part by Pró-Reitoria de Pesquisa da/UFAM (PRPq/UFAM) for additional research resources and for the grants for Master's and PhD's degrees. The review of this paper was arranged by Editor A. Lahav. *(Corresponding author: Eduardo Adriano Cotta.)*

A. S. Teixeira, Jr., and C. A. de Moraes Cruz are with the Department of Electronics and Computation, Universidade Federal do Amazonas, Manaus 69080-900, Brazil (e-mail: aldemir.junior.eng@gmail.com; agscruz@hotmail.com).

E. A. Cotta is with the Physics Department, Federal University of Amazonas (UFAM), Manaus 69080-900, Brazil (e-mail: cotta@ufam.edu.br).

D. W. de Lima Monteiro is with the Department of Electrical Engineering (DEE)/PPGEE, Universidade Federal de Minas Gerais, Belo Horizonte 31270-010, Brazil (e-mail: davies@ufmg.br).

Digital Object Identifier 10.1109/TED.2019.2911008

regions in a given CMOS process), many effects are unusual at room temperature, including material overstress, especially at interfaces, the changes in both charge-carrier mobility and availability, which affects silicon conductivity [9]. Such conditions directly affect the operation of silicon devices due to the changes in their properties, including threshold voltage, capacitances, current densities, and operational frequency. Thus, despite the existence of some specialized, proprietary and restricted CMOS process designed to operate in such extreme condition [10], standard CMOS technologies do not guarantee proper operation of circuits, especially those involving a large number of interdependent components, at these low temperatures. On the other hand, the literature shows that even in standard CMOS technologies, some basic circuit such as the APS keep reasonable operation below the freezeout temperature [3]. Few works, like [11], carry out investigations of pixels in the log mode against temperature. Even in this case, the temperature range analyzed is much higher than that presented and discussed in that paper. In addition, the focus in [11] concerns FPN investigations, whereas the present work focuses on temporal noise. However, these studies are still incipient, especially below 77 K. Moreover, in these papers, all of the data found regards CIS operating in the standard linear mode only.

The changes in temperature can affect the speed, power, and reliability of CMOS devices. In this sense, the purpose of this paper is to present a systematic analysis of the dynamic noise properties of a CMOS camera with 3T-APS technology in the logarithm mode at room (300 K, as reference), close to freezeout for silicon-based devices (100 K) and at cryogenic (30 K, below freezeout) temperatures. In each temperature, the pixels are submitted to three different light conditions: 1) darkness; 2) intermediate intensity (0.82 W/m^2); and 3) high intensity (9.15 W/m^2). Thus, a combination of these conditions can be analyzed simultaneously.

This paper is organized as follows. Section II describes the chip, setting configurations, and the detailed experimental setup. This is followed, in Section III, by an analysis of measurement results. Finally, Section IV presents the general conclusions.

II. Experimental Setup

The CIS in analysis in this paper consists of small array 8×8 pixels, as shown in detail in Fig. 1(a). The sensor has been fabricated in the AMS standard 4-metal 2-poly 0.35-μm CMOS process. Due to the silicon area limitation for this project, a larger array could not be implemented at this time.

The size of each pixel of the array is 10 μm $\times$ 10 μm and the fill factor of each pixel is 56%. The photodiode is an n$^+$-diffusion/p-sub diode with total area of 61 μm^2 and perimeter of 38.5 μm. Fig. 1(b) shows a schematic topology for each pixel. The transistors M1, M2, and M3, as well as the column amplifier M4, have the same dimensions: $W = 0.70$ μm and $L = 0.35$ μm. All pixels in a column share the same column amplifier transistor M4, and the same RST and reset-drain terminal (RDR) connections. Moreover, in a row, all pixels share the same SEL connection.

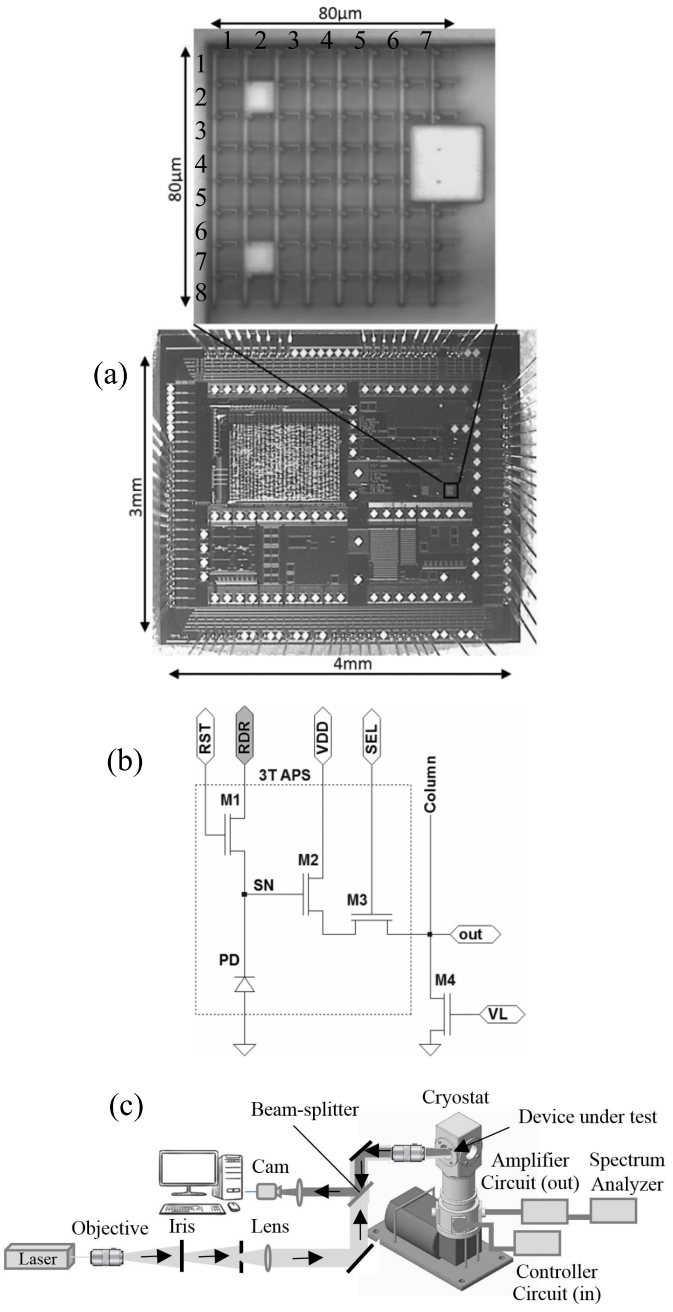

Fig. 1. (a) Microphotography of the fabricated chip with the designed 8×8 imager array and their respective dimensions. The numbers indicated above and beside of the pixel array identify the column and the row to map them. (b) Schematics of the three FET CMOS APS show the free RDR, reset (RST), row selection (SEL), and power supply (V_{DD}) connections. (c) Schematic experimental setup to optical experiments.

As the introduction of nonidealities during fabrication is a random process, it is not possible to predict either where it will take place in the array or its magnitude. Therefore, to guarantee that irregular photoresponse would be present in such a small array when illuminated by a flat light field, as column FPN, the nonidealities in photoresponse were, thus, intentionally implemented in the design, as discussed in [4] and [5]. Therefore, eight pixels with varying ratios of metal shielding (TiN/AlCu/TiN) were used for comparison, as can be observed in the inset of Fig. 1(a). Each pixel in the array

is identified by its (m, n) position, being the position (1, 1) that of the pixel in the upper left corner. Using the indications on this figure, we can verify that the pixels (2,2), (7,2), and (4,8) were totally covered. The pixels (3,7), (4,7), (5,7), (3,8), and (5,8) were partially covered for calibration purposes.

The image sensor was installed in a cold-finger closed cycle cryostat that enables temperature control from 300 down to 30 K. The pixel array was optically excited using the 514-nm line from an Ar^+ laser, with 5.4-mm beam diameter with circular profile in a uniform flat-field condition in three different intensities: 1) darkness; 2) low intensity (18 mW/m^2); and 3) high intensity (200 mW/m^2). The intensities chosen are due to the lower detection limit of the sensor ($\sim$10 mW/m^2) and above the saturation limit for the linear mode of operation ($\sim$150 mW/m^2). An optical setup consisting of two divergent lenses and diaphragms was used to produce the flat-field profile from the laser Gaussian profile. The area of the illuminated circle is more than 12 000 times bigger than that of the imager array. To verify the uniformity of the flat field, a small area was mapped in the center of the circle, around the region where the array was positioned. The mapped area is just four times bigger than that of the imager array. The mapping of the flat field was obtained by registering the voltage output of a single unaltered pixel of the array, pixel (1,1). The pixel was displaced in 10-μm steps using a translation stage with micrometric precision and the output voltage was registered with an average of 1000 samples for each point. The map of the field intensity profile does not show significant variations, being in the order of 0.6%. This confirms the uniformity of the field intensity to be delivered to the pixel array.

To remove external noise sources attributed to the power source and electromagnetic radiation, the electrical connections used a double-shielded cable. Moreover, the circuitry was enclosed in an aluminum box (2-mm wall thickness) and a combination of lithium-ion batteries is used as power supply. The control of the reading selection of the pixels and the operating mode was made manually in a printed circuit board using a jumpers set.

The signal measured in each pixel is amplified by an auxiliary circuit that presents three stages. The first stage has an instrumental amplifier with three internal amplifiers and good accuracy, low noise ($< 9\text{nV}/\sqrt{\text{Hz}}$), and high input impedance. The purposes of this stage are: 1) to mitigate the external noise removing signals in the common mode; 2) to give an ac coupling for the noise measured from image sensor removing the dc component (a limitation of the spectrum analyzer used); 3) to mitigate the imperfections of the cabling using a shield driver; and 4) to promote a lower limit for noise detection.

The in-amp used in the first stage presents high input impedance due to noninverting stages at its entrance. Therefore, when the input voltage, applied to the inverting input of the in-amp, is equal to noninverting input, the output voltage must be null. However, due to the introduction of nonidealities during the fabrication of these amplifiers, these input voltages normally are slightly different, resulting in a nonnull output voltage, the offset. Despite the availability of several circuits able to minimize the offset voltage, they generate a strong noise in the first stage increasing the lower limit for the temporal noise. Thus, a second stage was implemented in this project, where a first-order high-pass filter prevents that the offset be amplified by the subsequent stages. In this stage, a low-noise amplifier (LNA) was used (with about 0.8 nV/$\sqrt{\text{Hz}}$ of power spectrum). Thus, the noise contribution of this stage can be considered negligible.

The third, and last, stage was developed to both provide enough current for the low input impedance of the spectrum analyzer (using an LNA), as well as to limit the frequency response of the design through a low-pass filter. This frequency limitation will limit also the gain of the system, and consequently, the output voltage, protecting the spectrum analyzer (limited to 3.0 V_{rms}).

The noise generated by the cryostat and the compressor was removed using a differential amplifier, where the noise or drop voltage is rejected on the input stage, not been amplified by the amplifier circuit. Each spectrum presented in this paper is an average of 20 samples for each pixel individually and was limited by the maximum sampling allowed by the equipment.

The operation mode of the image sensor chosen to perform this analysis was the logarithmic mode. This choice was due to the small changes in the output voltage from the pixel, in contrast to the linear or lin–log modes. These changes, if too large, can generate a saturation of the output signal on the amplifier circuit, compromising the spectrum analyzer.

In the logarithmic mode, the circuit presents a dynamic range higher than 100 dB [3]–[5], [8]–[10], [12]. This is done using the pixel shown in Fig. 1(b) with the RDR and the RST terminals connected to V_{DD}. The most significant limitations of the APS operating in this mode include image distortions caused by FPN, image lag, and low sensitivity toward low illumination [1].

In our device, the logarithmic mode was generated connecting the RDR terminal permanently to V_{DD}. Instead of using an in-pixel current reference, the proposed technique applies an external voltage reference to the sense node (SN) through the RDR terminal.

The signal SN V_{out} presented in Fig. 2 is registered in logarithmic response using the RDR terminal set to V_{DD} for the temperatures and intensities of the incident light defined in this paper. The value for the sensor output voltage was determined by the average over all pixels, except the partially and completely shielded pixels given in Table I. In this figure, a clear reduction of the output voltage as the light intensity increases is observed. Moreover, the changes in the response for the same light intensity but at different temperatures are visible. In this case, a shift in the output signal is observed overall, not changing the curve shape, maintaining a certain linearity. These results are compliant to those observed and reported in [11] although within a different temperature range. This shift is due to the increase in the sensitivity of the device. The maintenance of the curve shape indicates that the response of the device is quite satisfactory for a wide range of temperatures, presenting the same behavior in all temperatures analyzed.

Concerning the behavior of completely shielded pixel in Fig. 2, as also shown in [4] and [5], the shielding is much more effective in the linear mode than in the logarithmic mode.

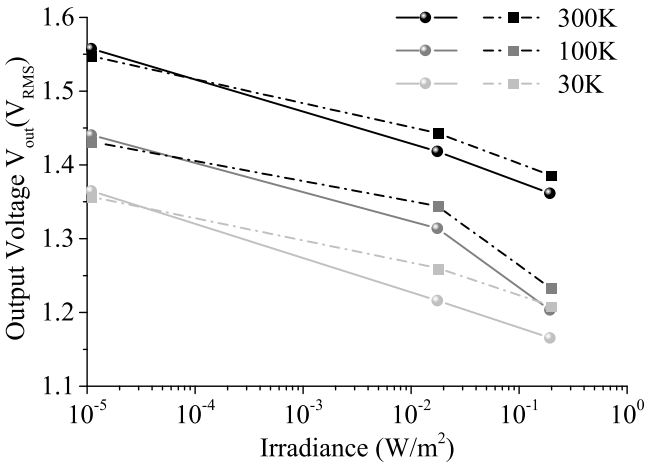

Fig. 2. Logarithmic SN response for the image sensor (filled circles) and the completely shielded pixel (4, 8) (filled squares) for different intensities (dark, 18 and 200 mW/m^2) and temperatures (30, 100, and 300 K). The output voltage for the array was determined by the mean value of all pixels, except the partially and fully shielded pixels. The continuous line (for the chip) and the dashed-dotted line [for the (4, 8) pixel] connecting the voltage points, for each temperature, are only meant to aid trend visualization.

TABLE I
ARRAY DESIGN CHARACTERISTICS AND SIGNAL CONTROL SETUP

Technology	0.35 µm, 2P4M CMOS
Pixel size	10x10 µm
Fill factor	56%
Fill factor of the covered pixels and their array positions (m,n)[a]	(2,2) = (7,2) = 2.3% (3,7) = 22.6% (4,7) = 17.3% (5,7) = 27.0% (3,8) = 14.4% (4,8) = 0.0% (5,8) = 20.7%
Array size	8×8
Signal control setup in logarithmic mode	
Supply voltage - V_{DD}	3.3 V – 3.6 V
Load Voltage – VL	1.0 V
Sampling time	20 s
Number of samples	20

[a] The respective position of the pixel in the array can be visualized in the inset of the Fig. 1(a).

Not only temperature but also illumination affects the response of pixel (4, 8), and this might be caused by crosstalk and/or laterally scattering of light. Due to such effects, it is much harder to use this kind of shielding to correct temperature-dependencies variations in regular pixels, as proposed in [11].

At 100 K, the sensor is analyzed close to the freezeout temperature (for silicon-based devices). To the temperatures above and below this region (intrinsic and partially ionized regions), it is expected that in the thermal equilibrium, for moderate and lightly doped (nondegenerate regime), the density of carriers decreases with the reduction in the temperature. Nevertheless, in this extrinsic region, the density of carriers is about stationary. Therefore, at high intensities of optical excitation, the nonionized dopants can be excited in excess to the conduction band. This increases the photocurrent generated by the sensor in relation to the other regimes promoting a reduction in V_{out}. This effect can be visualized in Fig. 2 (gray line), only for high intensity and for 100 K, where V_{out} presents a smooth curvature for low values.

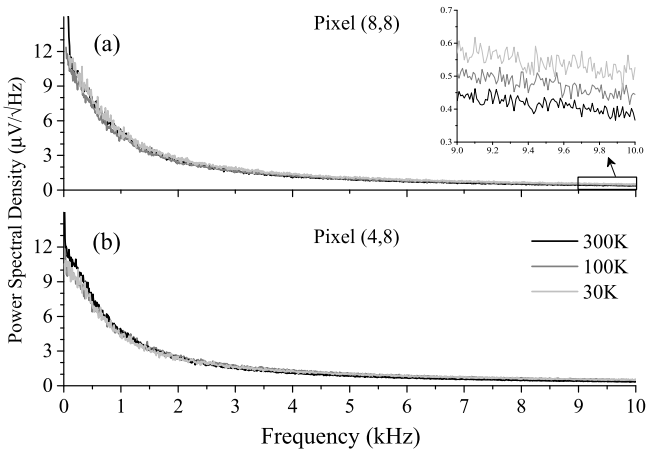

Fig. 3. Power spectral density for the pixels (a) (8, 8) and (b) (4, 8), all in dark condition. Each spectrum shows a superposition of the PSD for the three temperatures analyzed (300, 100, and 30 K) for comparison. The inset emphasizes the white noise region (between 9 and 10 kHz) distinguishing each plot.

Comparing the power spectrum density (PSD) of each pixel individually with the mean value of the whole array, under the same conditions (temperature, light intensity and excluding the total or partially covered pixels), a dispersion of values lower than 2% was identified. Thus, to compare the behavior between the pixels, three pixels have been chosen to represent each condition. Therefore, pixel (8,8) provides information about a totally exposed pixel and pixel (4,8) brings data of a fully covered one, regardless of the illumination condition to which the array is subjected. The ideal fill factor of the other eight different pixels, designed with metal shielding, varies according to the percentage of the covered area, and their values are indicated in Table I.

III. EXPERIMENTAL RESULTS AND DISCUSSION

Fig. 3 shows the PSD in dark condition for the three analyzed pixels, as indicated in the previous section, at the three temperatures considered. The magnitude of PSD found in this experiment is in agreement with the theoretical results estimated in [13]. In this condition, we observe that the PSD does not present significant changes for different temperatures. However, in the inset of Fig. 3(a), it is noted that the PSD level for high frequencies increases as temperature decreases. This behavior was found in all pixels, including those that are not shown here. This is completely opposite to what was expected because within this higher frequency range (much larger than corner frequency, f_c ~1.123 kHz), a predominance of the thermal noise and shot noise (white noises) is expected, which also increase with temperature.

It is known that thermal noise has an explicit dependence with temperature and the SN resistance. This is due to the fact of the node resistance is the combination of the nMOS M1 channel resistance and the photodiode series resistance. The node resistivity is inversely proportional to the product between the mobility and the carrier density at the transistor channel. At high temperatures (T), the mobility is limited by phonon scattering, being proportional to

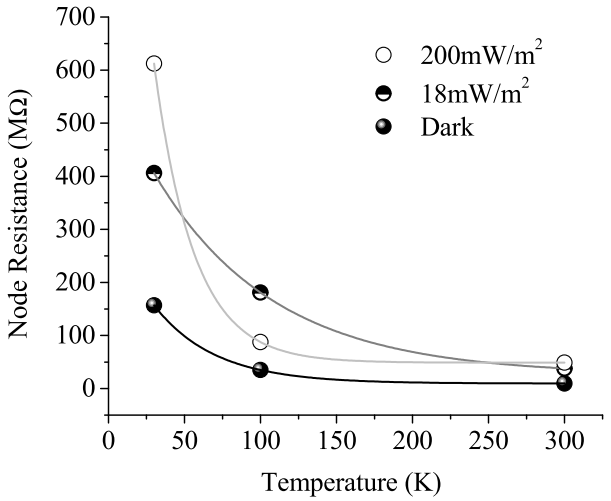

Fig. 4. Behavior of the pixel (8,8) for the node resistance (the continuous line is a fitting using an exponential curve).

$T^{-3/2}$, and therefore, the carrier density is proportional to $T^{(3/2)}\exp[-((E-E_F)/K_BT)]$, in which E is the carrier energy, E_F is the Fermi energy, and $K_B = 1.38\times10^{-23}$ J/K is Boltzmann's constant. Thus, the resistivity presents a decreasing exponential behavior with increasing temperature. This behavior in the node resistance provides a compensation effect in the thermal component of the noise, not being possible to separate them in the spectrum. However, in this case, the shot noise contribution is significantly lower in relation to the thermal contribution.

To confirm this behavior, Fig. 4 shows the corresponding value for the node resistance from pixel (8,8) for the three temperatures analyzed in each optical excitation condition. In this figure, it is clear that the exponential behavior for the node resistance by the curve fitting (continuous line) is in agreement with the previous discussion, showing that the increase in the light intensity changes significantly the node resistance. This leads one to believe that this behavior may have been induced by the carrier freezeout, once a trend is observed toward a stationary value for the node resistance above 100 K. These changes in the node resistance can explain the differences between the outputs voltages registered in Fig. 2 decreasing as the temperature decreases.

In Fig. 5, the PSD of the pixel (8,8) is presented for two optical excitation conditions (18 and 200 mW/m^2) for each temperature in analysis. In this measurement, we can identify an increase in the curve concavity as the light intensity increases, indicating an increase in the corner frequency. The corner frequency f_c in each case can be determined using a fitting on the PSD data (S_{rms}) to quantify the noise inside a frequency band between $f_{\max}$ and $f_{\min}$ using the expression

$$S_{\text{rms}}^2 = S_{\text{therm}}^2\left[f_c \ln\left(\frac{f_{\max}}{f_{\min}}\right) + (f_{\max} - f_{\min})\right] \quad (1)$$

in which S_{therm} is the thermal PSD to the noise at high frequencies. Equation (1) includes the flicker (first term) and thermal (second term) contributions for total noise, neglecting the shot noise contribution. We can verify that all parameters

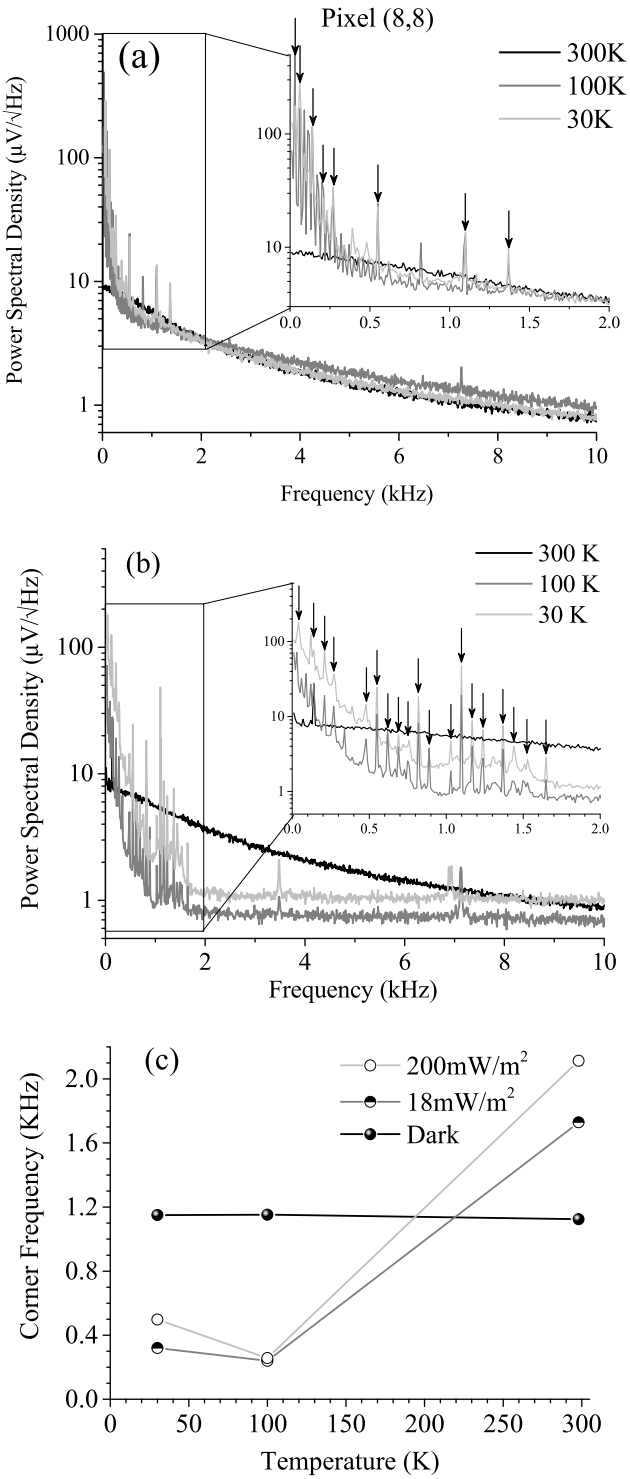

Fig. 5. PSD for the pixel (8,8). (a) Low intensity (18 mW/m^2) and (b) high intensity (200 mW/m^2) light excitation in logarithm scale. Each spectrum shows a superposition of the PSD for the three temperatures analyzed (300, 100, and 30 K) to comparison. The inset emphasize the low-frequency region ($f < f_c$). (c) Corner frequency (f_c) for 300, 100, and 30 K at different optical excitation conditions (dark, 18 and 200 mW/m^2) for the pixel (8,8) as function of the temperature.

are obtained experimentally, except f_c, being the unique adjust parameter for the fitting. Thus, in Fig. 5(c), we can verify the increase in f_c with temperature but only above the freezeout temperature. At low temperatures (below freezeout

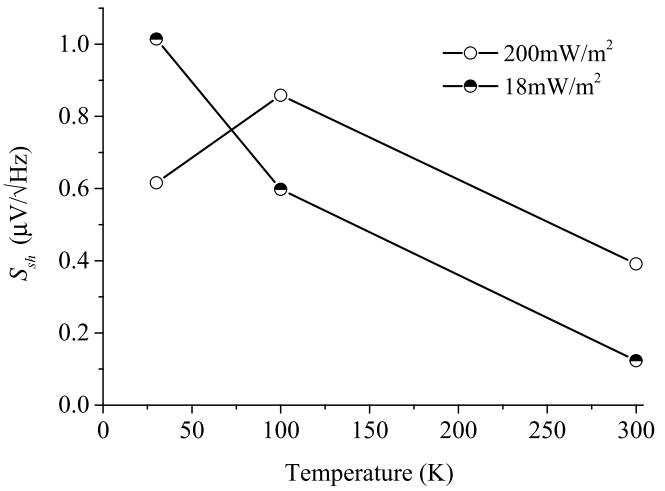

Fig. 6. Shot noise PSD (S_{sh}) contribution for the pixel (8,8) for the three temperatures in analysis when submitted to optical excitation.

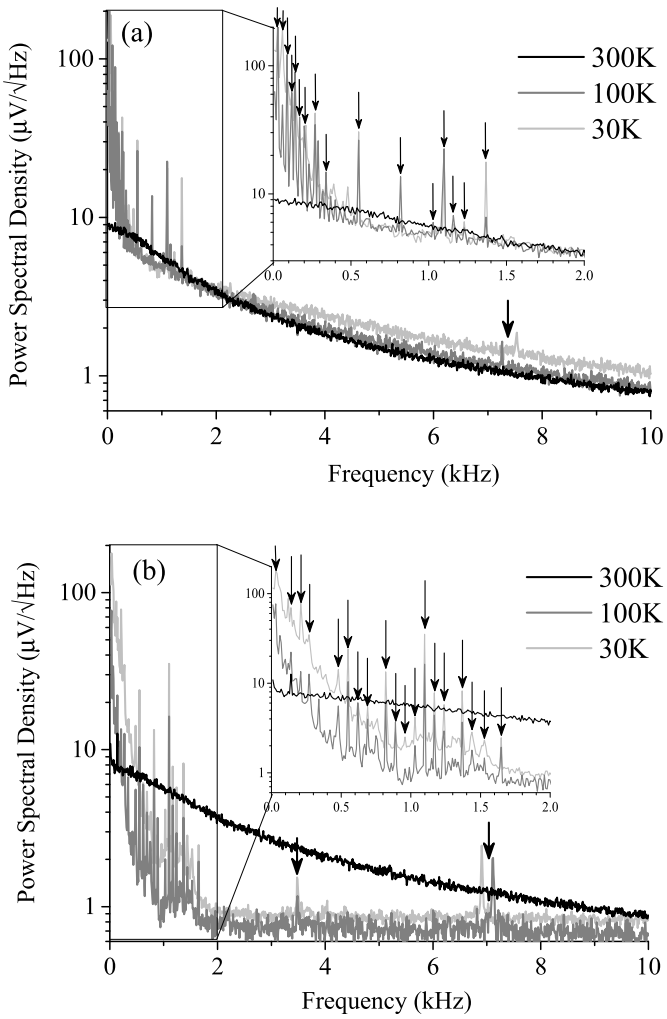

Fig. 7. PSD registered for the covered Pixel (4,8) subjected to (a) intermediate optical excitation (18 mW/m^2) and (b) high optical excitation (200 mW/m^2). The inset emphasize the "spikes" in the low-frequency region of the spectra.

temperature), f_c tends to a stationary value and lower than that found for 300K.

The corner frequency f_c is also a figure of merit to evaluate the flicker noise behavior, and generally, its reduction is irrelevant for high-speed cameras. However, it may affect their use for applications where a highly integrated time signal is present. It is known that f_c is a function of the temperature, bias, and device geometry as well as the fabrication process. In this case, its temperature dependence is directly linked to the node resistance. At dark condition, significant changes in the node resistance of the sensor are not observed and, consequently, in f_c, as indicated in Fig. 5(c). However, the large increase in the node resistance when the pixel is optically excited at low temperatures provides a reduction in the bias of the pixels and, consequently, a reduction in f_c.

At high frequencies, a competition between the shot and thermal noise is observed. Due to thermal stability of the system, this behavior seems to be exclusively due to the changes in the shot noise contribution. Shot noise is generally more sensitive to the effects of electron–electron interactions than the average conductance [14]. Therefore, an increase in the carrier density (and consequently the scattering process) can be induced by increasing the light intensity. Thus, the shot noise PSD (S_{sh}) contribution can be obtained subtracting the total PSD (S_{rms}) in high-frequency range from the dark condition (S_{therm}), so $S_{\text{rms}} = (S_{\text{sh}}^2 + S_{\text{therm}}^2)^{1/2}$. Therefore, in Fig. 6, we present the S_{sh} contribution for the three temperatures analyzed when the pixel (8,8) is optically excited. However, it is observed a reduction in S_{sh} as the temperature increases, a behavior opposite to the expected one. This could be induced by the increase in the node resistance for low temperatures, which is shown to be several orders of magnitude higher than the electron–electron scattering effect. This would also explain the reversal of this trend for temperatures lower than freezeout, which is observed both in S_{sh} as for the node resistance.

The main result presented in Fig. 5 is the presence of "spikes" at low temperatures (100 and 30 K). The intensity of these "spikes" is the several orders of magnitude higher than for a typical PSD output signal. For a good visualization, and comparison, the PSD shown in Fig. 5 was presented in log scale. The "spikes" are registered at low-frequency range (below f_c) and are not intermittent, i.e., they are found in the same frequency for both temperatures analyzed. The insets show in detail the spectral range where these "spikes" occur, and the arrows indicate some that appear in different temperatures but with the same frequency. The spectra for the other pixels present, qualitatively, the same characteristics of the (8,8) pixel, when submitted to the same condition (light intensity and temperature). This behavior can be interpreted as a signature of the pixel technology used and can be treated to identify the sensor.

The absence of the "spikes" at 300 K (above the freezeout temperature) indicates that the thermal energy is enough to break the binding energy of carriers in the traps related to the defects inside the gate oxide and at the oxide–silicon interface. These traps present different lifetimes (time in which the charge is trapped by the ion or defect in the lattice) due to its nature, so the charge emission occurs at specific rates. For low temperatures, the thermal energy is not enough to remove the charge from the trap but its lifetime allows that

each trap emits charges at a specific rate. Considering a trap distribution where different traps with different lifetimes can be found, it is possible to then identify a specific trap type in the PSD spectrum. This behavior is typical of random telegraph signal (RTS) noise, also known as popcorn or burst noise [15].

As indicated in Fig. 5(a) and (b), a "spike" is eventually registered in the high-frequency range. These isolated events can be associated with a weak trap (low energy binding), where the charge can be removed from the trap at a high rate. The PSD for the covered pixel (4,8) subjected to high and intermediate intensity light is presented in Fig. 7. In this figure, it is possible to identify the "spikes" with the same characteristics as those from the exposed pixel (Fig. 5). This observation can indicate three possibilities: 1) the first one indicating the presence of a cross talking among the fully capped pixel and adjacent pixels that receive light; 2) the second that may indicate that the part of the incident light has passed through the metal cap; or 3) the third, where simple part of the laterally scattered light may have reached the active part of the pixel. Whatever then, it is not possible to individually separate their contributions using this analysis, consisting in a topic yet to be studied. Moreover, the changes in the curve for different temperatures indicate that this pixel was optically excited. We attribute this to laterally scattered light that can excite the active region of the pixel.

IV. Conclusion

In this paper, we investigated the spectral behavior of the noise (the power spectrum density) generated by a CIS based on the 3T-APS technology under three different temperatures (300, 100, and 30 K) and three lighting conditions (dark, intermediate and high intensity) in the logarithmic mode (large dynamic range). These temperatures were chosen to be above, around, and below of the freezeout temperature for silicon devices for comparison. The PSD of the device in the range of 10 Hz and 10 kHz was registered. In this range, four types of noise sources were identified: flicker, thermal, shot noise, and RTS. The low intensity of the total noise (some μV_{rms}) for all temperatures analyzed is highlighted in this paper.

As expected, we identify a better performance of the device at low temperatures increasing the response of the image sensor but not necessarily reducing the total noise registered.

This anomalous behavior was investigated and attributed to the exponential increase of the node resistance for low temperatures. This effect was shown to be predominant mainly at high frequencies range (higher than corner frequency).

Moreover, "spikes" were registered in the PSD spectra in all pixels (including the covered) at low temperatures (below to freezeout temperature) and under light illumination. These spikes present a high intensity on the spectra, are intermittent in specific frequencies, and are present at a low-frequency range. We attribute these spikes to traps related to the defects inside the gate oxide and at the oxide–silicon interface. The rate in which the carriers get away the traps is inversely proportional to the binding energy of a given trap. Therefore, these spikes can be used to identify the quality of this region on the manufacturing process and as a fingerprint of the device.

Acknowledgment

The authors would like to thank P. N. A. Belmonte, V. Vecchia, R. A. de Souza, F. S. Torres, and L. P. Salles, for working intensively in the design of the chip.

References

[1] F. Serra-Graells, B. Misischi, E. Casanueva, C. Mendez, and L. Teres, "Low-power and compact CMOS APS circuits for hybrid cryogenic infrared fast imaging," *IEEE Trans. Circuits Syst. II, Exp. Briefs*, vol. 54, no. 12, pp. 1052–1056, Dec. 2007. doi: 10.1109/TCSII.2007.908873.

[2] S. M. Sze, *Semiconductor Devices: Physics and Technology*, 3rd ed. New York, NY, USA: Wiley, 2012, p. 39.

[3] P. V. F. do Rosário, L. P. Salles, A. S. B. de Mello, and D. W. de Lima Monteiro, "CMOS active-pixel sensor in low temperature," in *Proc. 29th Symp. Microelectron. Technol. Devices (SBMicro)*, Aracaju, Brazil, Oct. 2014, pp. 1–4. [Online]. Available: https://ieeexplore.ieee.org/document/6940114. doi: 10.1109/SBMicro.2014.6940114.

[4] C. A. de Moraes Cruz, D. W. de Lima Monteiro, E. A. Cotta, V. F. de Lucena, and A. K. P. Souza, "FPN attenuation by reset-drain actuation in the linear-logarithmic active pixel sensor," *IEEE Trans. Circuits Syst. I, Reg. Papers*, vol. 61, no. 10, pp. 2825–2833, Oct. 2014. doi: 10.1109/TCSI.2014.2327284.

[5] C. A. de Moraes Cruz, D. W. de Lima Monteiro, A. K. P. Souza, L. L. F. da Silva, D. R. de Sousa, and E. G. de Oliveira, "Voltage mode FPN calibration in the logarithmic CMOS imager," *IEEE Trans. Electron Devices*, vol. 62, no. 8, pp. 2528–2534, Aug. 2015. doi: 10.1109/TED.2015.2446992.

[6] H. Amhaz and G. Sicard, "A high output voltage swing logarithmic image sensor designed with on chip FPN reduction," in *Proc. 6th Conf. Ph.D. Res. Microelectron. Electron. (PRIME)*, Jul. 2010, pp. 1–4.

[7] E. Labonne, G. Sicard, and M. Renaudin, "An on-pixel FPN reduction method for a high dynamic range CMO S imager," in *Proc. 33rd Eur. Solid-State Circuits Conf. (ESSCIRC)*, Munich, Germany, Sep. 2007, pp. 332–335.

[8] B. Choubey, S. Aoyoma, S. Otim, D. Joseph, and S. Collins, "An electronic-calibration scheme for logarithmic CMOS pixels," *IEEE Sensors J.*, vol. 6, no. 4, pp. 950–956, Aug. 2006. doi: 10.1109/JSEN.2006.877983.

[9] S. Kavusi and A. El Gamal, "Quantitative study of high-dynamic-range image sensor architectures," *Proc. SPIE*, vol. 5301, pp. 1–12, Jun. 2004. doi: 10.1117/12.544517.

[10] S. B. Broadbent, "CMOS operation below freezeout," in *Proc. Workshop Low Temp. Semicond. Electron.*, Burlington, VT, USA, Aug. 1989. [Online]. Available: https://ieeexplore.ieee.org/document/50179. doi: 10.1109/LTSE.1989.50179.

[11] D. Joseph and S. Collins, "Temperature dependence of fixed pattern noise in logarithmic CMOS image sensors," *IEEE Trans. Instrum. Meas.*, vol. 58, no. 8, pp. 2503–2511, Aug. 2009. doi: 10.1109/TIM.2009.2014618.

[12] J. Lee, I. Baek, D. Yang, and K. Yang, "On-chip FPN calibration for a linear-logarithmic APS using two-step charge transfer," *IEEE Trans. Electron Devices*, vol. 60, no. 6, pp. 1989–1994, Jun. 2013. doi: 10.1109/TED.2013.2259236.

[13] H. Tian and A. El Gamal, "Analysis of 1/f noise in CMOS APS," *Proc. SPIE*, vol. 3965, pp. 1–9, May 2000. doi: 10.1117/12.385433.

[14] A. H. Steinbach, J. M. Martinis, and M. H. Devoret, "Observation of hot-electron shot noise in a metallic resistor," *Phys. Rev. Lett.*, vol. 76, no. 20, pp. 3806–3809, May 1996. doi: 10.1103/PhysRevLett.76.3806.

[15] A. Pelamatti, V. Goiffon, M. Estribeau, P. Cervantes, and P. Magnan, "Estimation and modeling of the full well capacity in pinned photodiode CMOS image sensors," *IEEE Electron Device Lett.*, vol. 34, no. 7, pp. 900–902, Jul. 2013. doi: 10.1109/LED.2013.2260523.